

# Simple, repeatable and low-cost SERS fibre probe for fluorochrome detection

Meijing Xia<sup>1,2</sup>, Hao Guo<sup>1,2</sup>, Jun Tang<sup>1,2</sup> ✉, Chunming Li<sup>1,2</sup>, Rui Zhao<sup>1,2</sup>, Lei Wang<sup>1,2</sup>, Wenyao Liu<sup>1,2</sup>, Jiangtao Yang<sup>1,2</sup>, Jun Liu<sup>1,2</sup>

<sup>1</sup>Science and Technology on Electronic Test & Measurement Laboratory, North University of China, Taiyuan 030051, Shanxi, People's Republic of China

<sup>2</sup>School of Instrument and Electronics, North University of China, Taiyuan 030051, Shanxi, People's Republic of China

✉ E-mail: tangjun@nuc.edu.cn

Published in Micro & Nano Letters; Received on 13th October 2017; Revised on 27th January 2018; Accepted on 2nd February 2018

A method for developing the spherical surface-enhanced Raman scattering (SERS) fibre probe is presented cladded with the silver nanoparticles to detect the fluorochrome molecular. By controlling the diameter of the fibre ball, the excellent SERS enhancement effect has been achieved up to about  $10^5$  due to the plasmonic silver nanoparticles, the coated parylene-C dielectric layer and the low-energy loss in the spherical resonant cavity. Meanwhile, the repeatability and stability of the fibre probe have been explored by coating the parylene-C with the error of 1%. It has proved an important superiority for potential commercial applications of this technique to detect the bio-molecular with the advantages of high sensitivity, high stability and low cost.

**1. Introduction:** Surface-enhanced Raman scattering (SERS) can enhance the intensity of Raman scattered signals of biomolecules absorbed on roughened metallic surfaces by a million fold. With the numerous unique advantages of molecular specificity, high sensitivity (down to single molecular level), simplicity of use and minimal photo-bleaching, SERS technology has been an effective way to detect the bio-molecules of the polluted river [1], the residues of the pesticides [2], the food additive [3] and so on. It has proved the excellent technology for rapid and non-destructive detection of chemical and biological substances.

Applying to explore the high-sensitivity SERS substrate, researchers have investigated fabrication methods for nano-structures. An ordered array of nanoparticles, nanowire and nanorods are widely found to develop the high-sensitivity SERS substrates. However, fabricating the well-ordered nano-structures are usually needed to complicate synthesis and expensive patterning technology such as focused ion beam and E-beam lithography.

Hence, more and more researchers have dedicated to develop a highly sensitive, ease of fabrication, portable and repeatable SERS substrate [4–8]. Liu *et al.* [5] have designed a portable fibre probe deposited with silver nanoparticles by laser-induced self-assembly method. The detection limit of the solution was  $10^{-10}$  M, and the repeatability error was <2.8%. Tang *et al.* [6, 7] developed the silver nano-wrinkles structures, and detection limit of R6G solution can be down to  $10^{-14}$  M with the detecting error was 2% after repeated 50 cycles. The same results have been achieved from the surface-enhanced fluorescence (SEF) effect [9, 10]. However, these technologies cannot be worked in the small space about sub- $\mu\text{m}$  and less portable.

The fibre tip has been reported to detect the bio-molecule in the small space with the high sensitivity, simple production process and low-cost [11]. Compared to the fibre tip, the spherically tipped fibre probe can focus the signal and enhance the signal intensity. It proves a potential SERS structure to detect the bio-molecule with the high sensitivity, high stability, low cost and portable.

This Letter presents the spherically tipped fibre probes based on the silver nanoparticles cladded with parylene-C for fluorochrome detection. The silver nanoparticles were deposited on the spherically tipped fibre probes with different diameters, and parylene-C was coated on the silver nanoparticles by vacuum vapour deposition system. On the basis of the theory of the energy loss [12] in the spherical resonant cavity, the high-sensitivity SERS substrate has been designed and fabricated. Besides, the spherically tipped fibre

probe coated with parylene-C has improved the repeatability and stability.

## 2. Experimental section

**2.1. Chemicals and materials:** Multimode fibre (IEC 60793-2-10, A1b) is purchased from Shanghai Hanyu Fiber Communication Technology Co., Ltd. Moreover, its cladding diameter, core diameter and numerical aperture are 125  $\mu\text{m}$ , 62.5  $\mu\text{m}$  and 0.27, respectively. Anhydrous ethanol (99.5%), hydrogen peroxide (30%), concentrated sulphuric acid (98%), isopropanol (99.7%), ammonia (28%), (3-aminopropyl) triethoxysilane (APTES) (98%), silver nitrate (99.8%), sodium citrate (97%) and rhodamine 6G (98%) are obtained from Aladdin Reagent Co., Ltd.

**2.2. Experimental setup:** As shown in Fig. 1a, the fibre probe was fixed, and the laser excited silver nanoparticles on the surface of the fibre ball transferring the fibre. Moreover, collecting the SERS signal at the end of the fibre ball. The Invia Renishaw Raman spectrometer is purchased from Renishaw, UK. The laser wavelength is 514.5 nm, the exposure time is 10 s and the power is 25  $\mu\text{W}$ .

**2.3. Preparation of the spherically tipped fibre probes:** The multimode spherical fibre was cut in the length of about 13 cm; coating layer of fibre end was peeled off in length of 2 cm and wiped with alcohol. The fibre probe was prepared by liquating the fibre end using the water hydrogen flame machine, as shown in Fig. 1b. The coating layer of the other end was peeled in length of 3 cm and connecting the Fibre Channel (FC) connector.

**2.4. Modification and characterisation of the spherically tipped fibre probe:** As shown in Fig. 1c, the spherically tipped fibre probe was modified by three steps. First of all, the 30% hydrogen peroxide was mixed with the 98% sulphuric acid at a volume ratio of 1:2, and the fibre probe was placed in the mixed solution for 30 min. Second, isopropyl alcohol with a concentration of 99.7% and ammonia with a concentration of 30% were mixed at a volume ratio of 9:1, and mixed again with the 98% APTES solution at a volume ratio of 9:1 to form the APTES system solution. Then, the hydroxylated fibre probe was placed in the APTES system solution for 120 min. The free molecules on the surface of the fibre probe would be rinsed with the deionised water. Finally, the silver sol solution was prepared by the

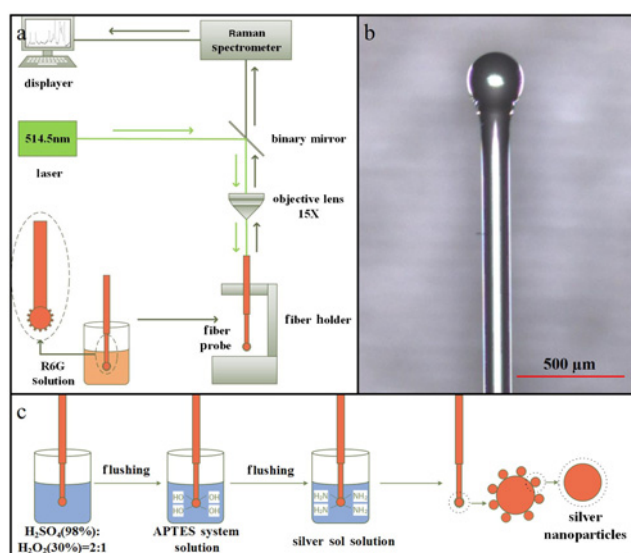


**Fig. 1** Experimental setup

*a* Schematic diagram of system detection setup

*b* Spherically tipped fibre probe observed under a confocal microscope

*c* Modification process of fibre probe

classical Lee and Meisel [13] chemical heating method, and the fibre probe was placed in the silver sol solution for 30 min. The morphology of the silver nanoparticles on the surface of the spherically tipped fibre probe was characterised by scanning electron microscopy (SEM) (SUPRA 55 SAPPHERE, Carl Zeiss AG, Jena, Germany). In addition, the enhancement effect of silver nanoparticles was observed by fluorescence microscopy (BX53M, Olympus, Japan).

**2.5. SERS activity detection of the spherically tipped fibre probes:** About 30 ml R6G with a concentration of  $10^{-5}$  mol/l was used to investigate the SEF and SERS effects. R6G is the widely used probe in the field of SERS activity testing with the advantage of stable property and strong SERS activity. The spherically tipped fibre probe was immersed in the prepared R6G solution for 30 s and dried in air, then fixed it on the fibre holder for SERS activity detection. Here, the Raman characteristic peak of R6G molecules at  $1650\text{ cm}^{-1}$  is well known caused by the stretching vibration of the C–C bond. The 50 nm thick parylene-C film was cladding on the silver nanoparticles of the fibre probe to investigate the repeatability of the fibre probe. The parylene-C film was deposited by the Parylene Deposition System (PDS) 2010 Labcoter parylene deposition system purchased from Specialty Coating Systems, Inc. (USA). In this work, the parylene-C film was about 50 nm using the polychlorinated dimethylbenzene particles in the weight of 80 mg with the temperature of  $25^{\circ}\text{C}$  and pressure of 25 mTorr.

**3. Results and discussion:** Fig. 2 shows the morphology characterisation of the silver nanoparticles on the surface of the spherically tipped fibre probe. After assembled in the time of 30 min, the silver nanoparticles are distributed on the surface of the spherically tipped fibre probe with the range of sizes from 40 to 100 nm, as shown in Fig. 2b.

The spherically tipped fibre probes coated and un-coated silver nanoparticles were immersed in the R6G solution for 30 s. Moreover, the SEF effect of the silver nanoparticles was achieved using the fluorescence microscope. As shown in Fig. 3, the morphology and the fluorescence characterisation of the spherically tipped fibre probe have been observed. In our experiment, the fibre probes coated and un-coated the silver nanoparticles were excited by the

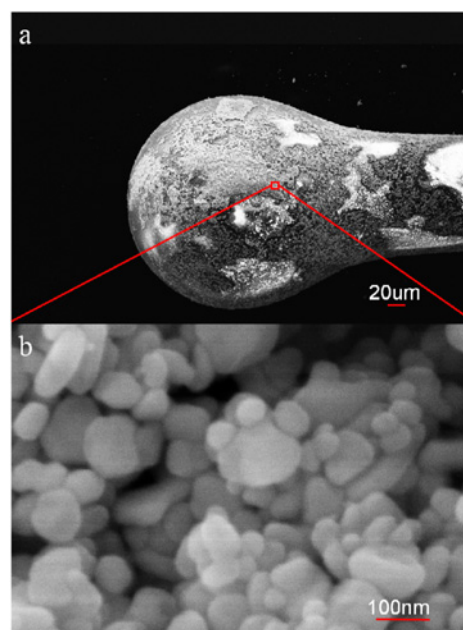


**Fig. 2** SEM characterisation of silver nanoparticles on the fibre probe

*a* Spherically-tipped fibre probe coated with silver nanoparticles observed under SEM with the magnification of 222 X

*b* Spherically-tipped fibre probe coated with silver nanoparticles observed under SEM with the magnification of 130 KX

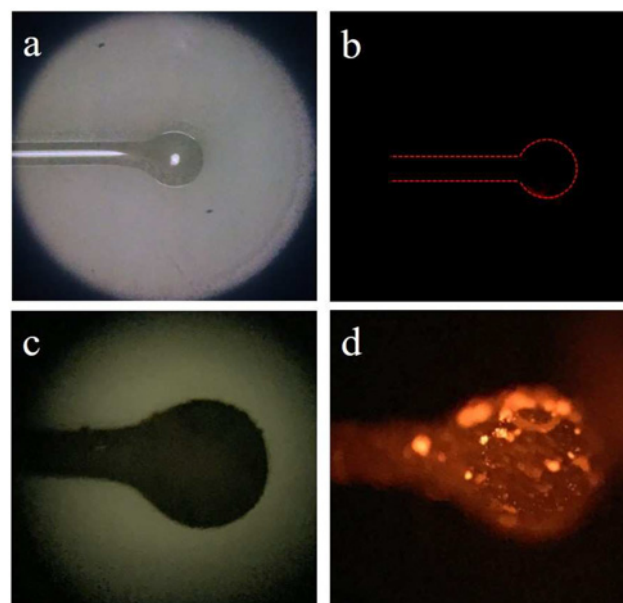


**Fig. 3** Morphology and the fluorescence characterisation of the spherically tipped fibre probe

*a* Morphology characterisation of the spherically tipped fibre probe without silver nanoparticles under bright field state

*b* Fluorescence characterisation of the R6G-spherically tipped fibre probe without silver nanoparticles under laser excitation

*c* Morphology characterisation of the spherically tipped fibre probe with silver nanoparticles under bright field state

*d* Fluorescence characterisation of the R6G-spherically tipped fibre probe with silver nanoparticles under laser excitation

green laser, and the corresponding fluorescence phenomenon has been shown in Figs. 3b and d. With the silver nanoparticles, the spherically tipped fibre probes generate stronger red fluorescence, by comparing with the spherically tipped fibre probes un-coated silver nanoparticles. The R6G molecular can be earlier detected using the spherically tipped fibre probes coated with the silver nanoparticles caused by the SEF effect.

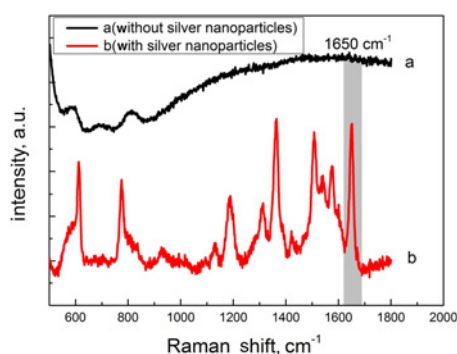


**Fig. 4** Raman spectra of R6G molecules that is measured by fibre probe with and without silver nanoparticles

Fig. 4a shows the Raman spectra of R6G detected by the fibre probe. There are not any Raman signals detected by the fibre probe that un-coated the silver nanoparticles. In comparison, the stronger Raman signals have been achieved using the probe coated with the silver nanoparticles because of the localised surface plasmon resonance effect [14]. The intensity of the fibre Raman background is very weak compared with that of the excitation laser, which has been reduced by the ways by the method of other reports [15–17]. The Raman background noise of the fibre has been reduced to get the stronger Raman signal of R6G molecule. Moreover, then the Raman spectrum was obtained after removing Raman background noise as the curve ‘b’ shown in Fig. 4.

The enhancement factor (EF) of the silver nanoparticles was measured by the ratio of Raman signal intensity of R6G molecule as follows:

$$EF = \frac{I_{SERS}}{N_{SERS}} \bigg/ \frac{I_{RS}}{N_{RS}} = \frac{I_{SERS}}{I_{RS}} \frac{N_{RS}}{N_{SERS}} \quad (1)$$

where  $I_{SERS}$  and  $I_{RS}$  are severally the SERS signal integral intensity of R6G molecule on the fibre probe that coated and un-coated the silver nanoparticles. The  $N_{SERS}$  and  $N_{RS}$  are the amount of R6G molecules for the two kinds of fibre probes, respectively. In addition, the value of  $I_{RS}$  cannot be obtained, because the Raman signal of the fibre probe that un-coated the silver nanoparticles were hard to achieve. However, the intensity of the Raman signal and the fluorescence signal was proportional to the area of scattering cross-section as follows [18]:

$$\frac{I_{RS}}{I_{Fluo}} \simeq \frac{\sigma_{RS}}{\sigma_{Fluo}} \quad (2)$$

The  $\sigma_{RS}$  and  $\sigma_{Fluo}$  are the scattering cross-sectional areas of the Raman signal and the fluorescence signal, respectively, and  $I_{Fluo}$  is the fluorescence signal intensity of R6G molecule on the fibre probe with silver nanoparticle deposited. Combining (1), the EF of silver nanoparticles is as below:

$$EF \simeq \frac{I_{SERS}}{I_{Fluo}} \frac{\sigma_{Fluo}}{\sigma_{RS}} \frac{N_{Fluo}}{N_{SERS}} \quad (3)$$

According to the method reported in the literature [19], the fluorescence signal integral intensity of the curve ‘a’ in Fig. 4 was 540,201, and the SERS signal integral intensity of the curve ‘b’ in Fig. 4 was 135,283. The scattering cross-sectional areas of the Raman signal and the fluorescence signal of R6G molecular are  $\sim 2.6 \times 10^{-22}$  and  $\sim 10^{-16}$  cm<sup>2</sup>, respectively [20].  $N_{Fluo}$  and  $N_{SERS}$  are the number of R6G molecules in the scattering volume of the

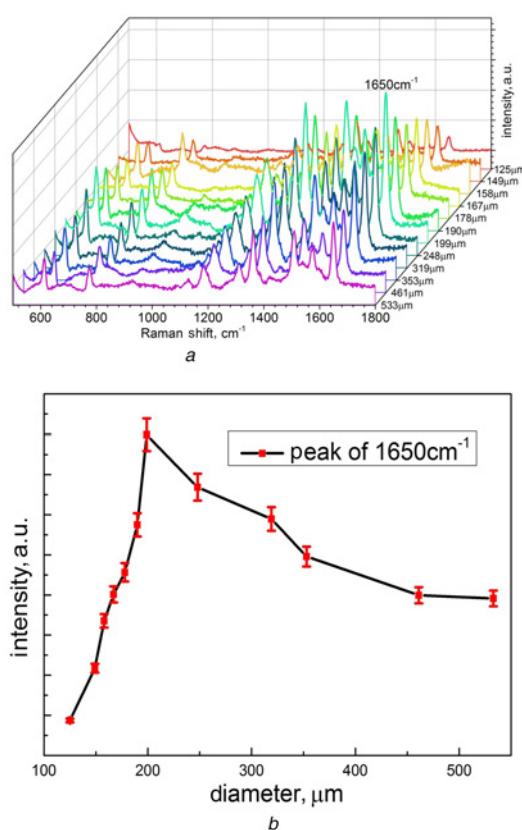


**Fig. 5** SERS effect of the probe

a SERS enhancement effect detection of the spherically tipped fibre probe with a different diameter

b Abscissa in this figure indicates the diameter of the spherical fibre, the ordinate represents peak height of R6G molecules at 1650 cm<sup>-1</sup>

two kinds of fibre probe. The EF of the silver nanoparticles was about  $9.6 \times 10^4$  based on the above parameters and formula (3) [21].

The SERS effect of the probe was determined as a function of the diameter of the probe sphere as depicted in Fig. 5. The enhancement effect was the strongest with the fibre ball diameter of around 200 μm.

Theoretically, with increasing diameter of the fibre ball, the capacity of storing light improves and the light loss increases. Also, due to the advantages of the aggregation effect, there were more lights that can be aggregated by increasing the diameter of the fibre ball. However, there is energy loss in the spherical resonant cavity. The quality factor ( $Q$ ) is an important parameter of the spherical resonant cavity and it represents the storage capacity of the light to couple into the cavity. The relational expression was calculated by (4) in which radiation loss ( $Q_{\text{radiation}}$ ), absorption loss ( $Q_{\text{absorption}}$ ), and scattering loss ( $Q_{\text{scattering}}$ ) are three influencing factors of  $Q$  value [12, 22]

$$\frac{1}{Q} = \frac{1}{Q_{\text{radiation}}} + \frac{1}{Q_{\text{absorption}}} + \frac{1}{Q_{\text{scattering}}} \quad (4)$$

Radiation loss, also named bending loss, increases exponentially with increasing diameter, and its effect on  $Q$  value can be neglected on condition that  $D/\lambda > 15$  and  $Q_{\text{radiation}} > 10^{11}$  [22]. The wavelength ( $\lambda$ ) of the incident light is 514.5 nm, so the effect on  $Q$  value of the radiation loss can be ignored as long as  $D > 7.7175$  μm. Hence, the effect of the radiation loss can be ignored with the diameter of fibre ball ranges from 180 to 600 μm here. The absorption loss was only dependent on the property of the material. Hence, the impact of  $Q_{\text{scattering}}$  was the only factor to be considered.

$Q_{\text{scattering}}$  is the light scattering energy dissipation caused by the surface roughness of the microsphere resonator, which is dependent on the diameter and the roughness of the fibre ball as follows:

$$Q_{\text{scattering}} = \frac{3\lambda^2 l^{10/3}}{16\pi^5 \sigma^2 n_{\text{eff}}^2 q^{5/2}} \quad (5)$$

Here,  $l = n_{\text{eff}} \dots \pi \dots D/\lambda$ , where  $D$  is the diameter of the fibre ball,  $n_{\text{eff}}$  is the effective refractive index of the fibre ball,  $\lambda$  is the wavelength of the incident light,  $\sigma$  is the surface roughness of the fibre ball, and  $q$  is the resonant mode order. In this work,  $n_{\text{eff}} = 1.408$  and  $\lambda = 514.5$  nm, assuming  $q = 1$  [23]. The theoretical relationship between  $Q_{\text{scattering}}$  and the cavity diameter can be obtained when the diameter was ranging from 100 to 600  $\mu\text{m}$  and the surface roughness  $\sigma$  was about 50 nm, as shown in Fig. 6a. It can be seen that  $Q_{\text{scattering}}$  increases with increasing diameter from Fig. 6a. So,  $Q$  also increases with increasing the diameter of the fibre ball according to (4). Similarly, the theoretical relationship between  $Q_{\text{scattering}}$  and the surface roughness  $\sigma$  can be obtained when the surface roughness  $\sigma$  was ranging from 0 to 200 nm and the cavity diameter was valued to 200  $\mu\text{m}$ , as shown in Fig. 6b. It can be obtained that  $Q_{\text{scattering}}$  decreases with increasing surface roughness from Fig. 6b. So,  $Q$  also decreases with increasing the surface roughness of the fibre ball by (4). The surface roughness increases with the increase of the diameter of the fibre ball [24].

The parylene-C with the thickness of 50 nm was cladded on the surface of the fibre probe as shown in Fig. 7a. Parylene-C has been widely used in the bio-microelectromechanical system field due to the advantages of well biocompatibility, optical transparency, chemical inertness, and hydrophobicity [25]. Meanwhile,

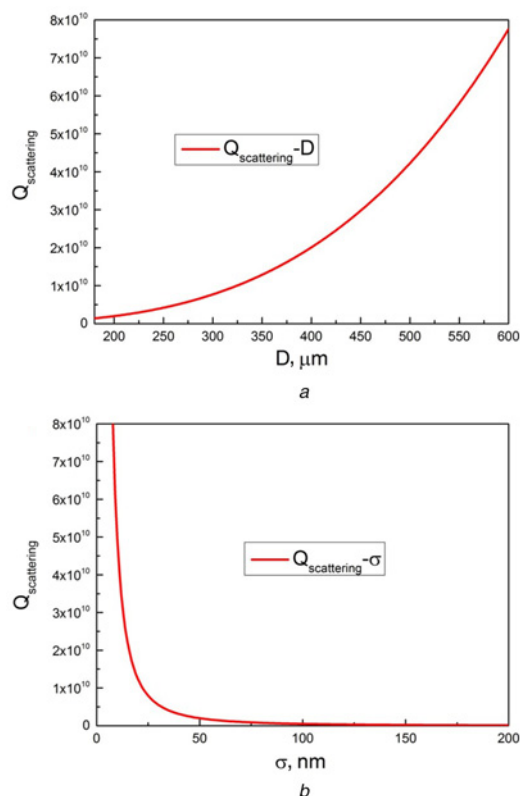


**Fig. 6** Theoretical relationship between  $Q_{\text{scattering}}$  and the cavity parameters

a Simulation diagram between  $Q_{\text{scattering}}$  and the diameter  $D$  of the fibre ball  
b Simulation diagram between  $Q_{\text{scattering}}$  and the surface roughness  $\sigma$  of the fibre ball

parylene-C could protect the silver nanoparticles on the fibre probe against the R6G molecules to improve the repeatability. Comparing Figs. 7b and c, it can be obtained that the repeatability of the fibre probe cladded with parylene-C is better than the fibre probe without parylene-C. The standard error of the former was about 1% and the latter was about 65% from Fig. 7d. It has

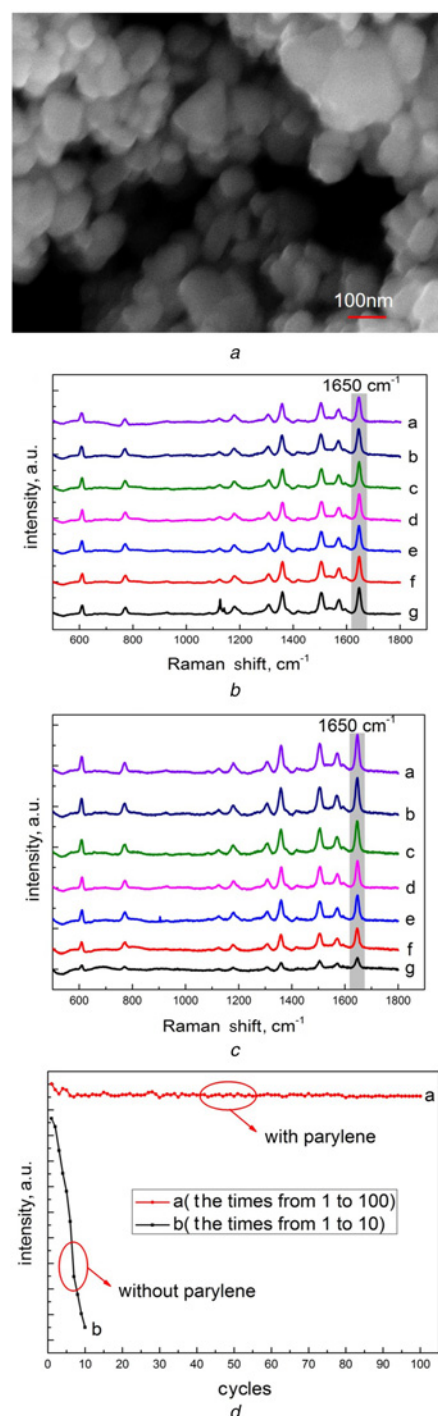


**Fig. 7** Parylene-C with the thickness of 50 nm

a SEM characterisation of the silver nanoparticles cladded with parylene-C of the thickness of 50 nm on fibre probe

b Repeatability detection of the fibre probe with deposition of parylene-C  
c Repeatability detection of the fibre probe without deposition of the parylene-C

d Repeatability detection trend of the fibre probe with and without depositions of the parylene-C

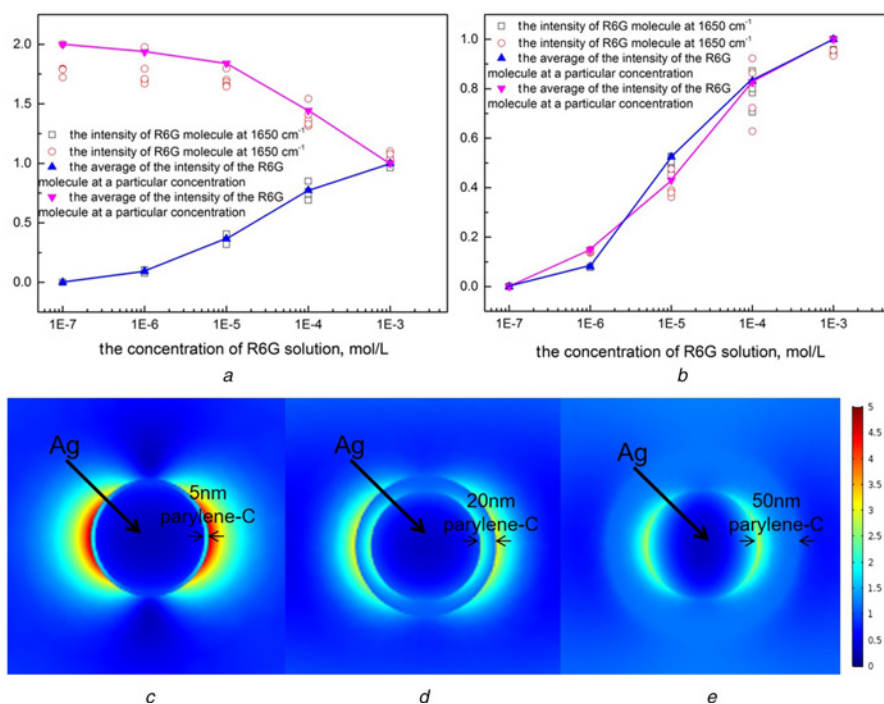


**Fig. 8** Electromagnetic enhance effects

*a, b* Normalise to [0, 1] of the SERS detecting tendency of the fibre probe without and with parylene-C, respectively

*c, d, e* Electromagnetic simulations obtained from XFDTD calculations at wavelength 514.5 nm of one silver nanoparticle with 70 nm diameter with 5, 20, and 50 nm parylene-C on the fibre probe, respectively

proved the well repeatability of the fibre probes cladded by parylene-C.

Figs. 8c–e show the electromagnetic enhanced effects for the silver nanoparticle cladding with the parylene-C thicknesses of 5, 20, and 50 nm simulated by the XFDTD software. The intensity of the electromagnetic field is weakened with the increase in the thickness of parylene-C. Meanwhile, the corresponding Raman enhance effect has been investigated. The blue curves in Figs. 8a and b indicate that the SERS detecting tendency of the fibre probe without and with parylene-C from low concentration to the high concentration of the R6G solution, respectively. The variation tendency of the SERS effect for the fibre probe without and with parylene-C rises with increasing the concentration of the R6G solution. The magenta curves represent that the results from high concentration to the low concentration of the R6G solution. It is clear that the SERS effect of the fibre probe without parylene-C deposited is still enhanced as the concentration decreases. Owing to the vestigial of R6G molecules on the surface of the probe after the fibre was flushed with alcohol and deionised water. However, after cladding the parylene-C, there are little R6G molecules remaining on the probe surface after flushed with alcohol and deionised water. It proves fibre probes cladding with parylene-C can improve the repeatability. In general, the SERS effect of the fibre probe cladding with parylene-C will be weakened, but the repeatability can be improved. It has the advantages of high repeatability, high stability, and low cost.

**4. Conclusion:** In this work, a spherical SERS fibre probe has been fabricated by coating the silver nanoparticles. By controlling the diameter of fibre spherical to 200  $\mu\text{m}$ , the SERS effect has been enhanced up to  $9.6 \times 10^4$  to detect the R6G molecular. Meanwhile, the parylene-C film had been cladded on the probe acts as a protective layer, and the repeatability error was about 1%. This fibre probe has good application prospect in the molecule detection field such as the detection of pesticide residues in the polluted river, the biochemical molecule in the

food and medical science, and so on. Moreover in future, it is expected that this fibre probe can be used for single molecule detection with the advantage of simple, reusable, and low cost.

**5. Acknowledgments:** We acknowledge the financial support from the Natural Science Foundation of China (grant nos. 51635011, 51727808, and 61640601) and the Shanxi ‘1331 Project’ Key Subjects Construction.

## 6 References

- [1] Caballero-Díaz E., Simonet B.M., Valcárcel M.: ‘Microextraction by packed sorbents combined with surface-enhanced Raman spectroscopy for determination of musk ketone in river water’, *Anal. Bioanal. Chem.*, 2013, **405**, pp. 7251–7257
- [2] Yang T.X., Zhao B., Kinchla A.J., *ET AL.*: ‘Investigation of pesticide penetration and persistence on harvested and live basil leaves using surface-enhanced Raman scattering mapping’, *J. Agric. Food Chem.*, 2017, **65**, pp. 3541–3550
- [3] Weidemaiera K., Carruthers E., Curry A., *ET AL.*: ‘Real-time pathogen monitoring during enrichment: a novel nanotechnology-based approach to food safety testing’, *Int. J. Food Microbiol.*, 2015, **198**, pp. 19–27
- [4] Liu J.W., Wang J.L., Huang W.R., *ET AL.*: ‘Ordering Ag nanowire arrays by a glass capillary: a portable, reusable and durable SERS substrate’, *Sci. Rep.*, 2012, **2**, p. 987
- [5] Liu Y., Huang Z.L., Zhou F., *ET AL.*: ‘Highly sensitive fiber surface-enhanced Raman scattering probes fabricated using laser-induced self-assembly in a meniscus’, *Nanoscale*, 2016, **8**, pp. 10607–10614
- [6] Tang J., Guo H., Chen M., *ET AL.*: ‘Wrinkled Ag nanostructured gratings towards single molecule detection by ultrahigh surface Raman scattering enhancement’, *Sens. Actuators B*, 2015, **218**, pp. 145–151
- [7] Tang J., Guo H., Zhao M.M., *ET AL.*: ‘Ag nanoparticles cladded with parylene for high-stability microfluidic surface-enhanced Raman scattering (SERS) biochemical sensing’, *Sens. Actuators B*, 2017, **242**, pp. 1171–1176
- [8] Cao J., Wang J.Z.: ‘Development of Ag nanopolyhedra based fiber-optic probes for high performance SERS detection’, *New J. Chem.*, 2015, **39**, pp. 2421–2424

- [9] Zhang X.F., Kong X.M., Lv Z.P., *ET AL.*: 'Bifunctional quantum dot-decorated Ag@SiO<sub>2</sub> nanostructures for simultaneous immunoassays of surface-enhanced Raman scattering (SERS) and surface-enhanced fluorescence (SEF)', *J. Mater. Chem. B.*, 2013, **1**, pp. 2198–2204
- [10] Wei Q.S., Acuna G., Kim S., *ET AL.*: 'Plasmonics enhanced smart-phone fluorescence microscopy', *Sci. Rep.*, 2017, **7**, p. 2124
- [11] Atie E.M., Xie Z., Eter A.E., *ET AL.*: 'Remote optical sensing on the nanometer scale with a bowtie aperture nano-antenna on a fiber tip of scanning near-field optical microscopy', *Appl. Phys. Lett.*, 2015, **106**, p. 641
- [12] Ling T., Chen S.L., Guo L.J.: 'Fabrication and characterization of high Q polymer micro-ring resonator and its application as a sensitive ultrasonic detector', *Opt. Express.*, 2011, **19**, pp. 861–869
- [13] Zhu Q.X., Li H., Lu F., *ET AL.*: 'A widely applicable silver sol for TLC detection with rich and stable SERS features', *Nanoscale Res. Lett.*, 2016, **11**, pp. 1–8
- [14] Li C.T., Chen H.F., Un L.W., *ET AL.*: 'Study of optical phase transduction on localized surface plasmon resonance for ultrasensitive detection', *Opt. Express*, 2012, **20**, pp. 3250–3260
- [15] Ma J.Y., Li Y.S.: 'Fiber Raman background study and its application in setting up optical fiber Raman probes', *Appl. Opt.*, 1996, **35**, pp. 2527–2533
- [16] Cooney T.F., Schoen C.L., Sharma S.K., *ET AL.*: 'Rare-earth-doped glass fiber for background rejection in remote fiber-optic Raman probes: theory and analysis of holmium-bearing glass', *Appl. Spectrosc.*, 1993, **47**, pp. 1683–1692
- [17] Myrick M.L., Angel S.M.: 'Elimination of background in fiber-optic Raman measurements', *Appl. Spectrosc.*, 1990, **44**, pp. 565–570
- [18] Xie Z.G., Tao J., Lu Y.H., *ET AL.*: 'Polymer optical fiber SERS sensor with gold nanorods', *Opt. Commun.*, 2009, **282**, pp. 439–442
- [19] Etchegoina P.G., Le Ru E.C.: 'A perspective on single molecule SERS: current status and future challenges', *Phys. Chem. Chem. Phys.*, 2008, **10**, pp. 6079–6089
- [20] Shim S., Stuart C.M., Mathies R.A.: 'Resonance Raman cross-sections and vibronic analysis of rhodamine 6G from broadband stimulated Raman spectroscopy', *ChemPhysChem*, 2008, **9**, pp. 697–699
- [21] Wang T., Zhang Z.S., Liao F., *ET AL.*: 'The effect of dielectric constants on noble metal/semiconductor SERS enhancement: FDTD simulation and experiment validation of Ag/Ge and Ag/Si substrates', *Sci. Rep.*, 2014, **4**, p. 4052
- [22] Liu J.H., Tang J., Shang C.L., *ET AL.*: 'Optimization of microsphere's DQ product based on resonant micro-optical gyro', *Acta Phys. Sin.*, 2015, **64**, p. 154206
- [23] Vernoooy D.W., Ilchenko V.S., Mabuchi H., *ET AL.*: 'High-Q measurements of fused-silica microspheres in the near infrared', *Opt. Lett.*, 1998, **23**, pp. 247–279
- [24] Milleret V., Hefti T., Hall H., *ET AL.*: 'Influence of the fiber diameter and surface roughness of electrospun vascular grafts on blood activation', *Acta. Biomater.*, 2012, **8**, pp. 4349–4356
- [25] Kim B.J., Meng E.: 'Micromachining of parylene-C for bioMEMS', *Polym. Adv. Technol.*, 2016, **27**, pp. 564–576